

# Single-Source Precursor Synthesis of a Compositionally Complex Early Transitional Metal Carbonitride (Ti,Zr,Hf,Nb,Ta) $N_xC_{1-x}$

Dharma Teja Teppala, Jan Bernauer, Aasir Rashid, Milan Pejic, Dejan Zagorac, Branko Matovic, and Emanuel Ionescu\*

Compositionally complex transitional metal nitrides are possible candidates for ultra-high temperature usage and are known for their superior properties due to the high configuration entropy. It is often difficult to synthesize pure metal nitrides in bulk, due to significant oxygen contamination; hence, they are synthesized mainly as thin films through magnetron sputtering, chemical vapor deposition or surface nitridation of high entropy alloys. The present article reports on a single-phase compositionally complex ceramic, i.e.,  $(Ti_{0.2}Zr_{0.2}Hf_{0.2}Nb_{0.2}Ta_{0.2})N_xC_{1-x}$ , that is synthesized for the first time by employing an organometallic precursor route and using a double ammonolysis process. A multidisciplinary approach is performed to study these compositionally complex nitride and carbonitride systems, including experimental and theoretical investigations.

## 1. Introduction

Multi-principal element alloys are solid solutions containing multiple metallic species in their crystalline structure, mostly in near equiatomic ratio between 5 and 35 at%. Yeh et al.<sup>[1]</sup> have synthesized the multi-principal element alloy  $Al_xCoCrFeCuNi$ , and Cantor et al.<sup>[2]</sup> first reported multi-principal element alloys, i.e.,  $CoCrFeMnNi$ ,<sup>[2]</sup> although later the term high entropy

materials were used frequently. The alloys were classified based on their configuration entropy  $\Delta S_{mix} = -R \sum_{i=1}^n x_i \ln x_i$  into low-entropy ( $\Delta S_{mix} \leq 0.69R$ ), medium-entropy ( $0.69R \leq \Delta S_{mix} \leq 1.61R$ ) and high-entropy ( $\Delta S_{mix} \geq 1.61R$ ) formulations.<sup>[1]</sup> Typically, the number of elements  $n$  is assumed to be  $\geq 5$  to consider alloys as high-entropy alloys. The mixing entropy calculations were made on the assumption of complete random mixing with no clustering; however, the value is lower than calculated since the interactions between the constituents are not ideal and constitute short-range ordering.<sup>[3,4]</sup> Aside from Hume-Rothery rules, configurational entropy is


one of many indicators that can be used to assess the high entropic nature of multi-principal element alloys.<sup>[5]</sup> Also, other parameters, such as the valence electronic concentration (VEC), were considered valuable descriptors to rationalize whether compositionally complex alloys may form as single-phase compounds and whether those alloys are stabilized solely based on (configurational) entropy.<sup>[2,6]</sup>

As the concept was extended to ceramics, where the ceramics consist of cationic and anionic sublattices occupied by metallic cations and non-metallic anions, the increase in disorder in either one or both of the sublattices increases the configurational entropy of the ceramic, thus favoring the formation of single-phase ceramic compounds. However, currently, the alloys and ceramics are classified as medium entropy with  $R \leq \Delta S_{mix} \leq 1.5R$  and high entropy with  $\Delta S_{mix} \geq 1.5R$  and are being considered widely as the basis of classification.<sup>[4]</sup> Rost et al. successfully synthesized a rock-salt type oxide  $(Mg_{0.2}Ni_{0.2}Co_{0.2}Cu_{0.2}Zn_{0.2})O$  as a bulk sample, which was also entropy-stabilized.<sup>[7]</sup> Subsequently, many other non-equimolar and equimolar compositions such as  $Sr((Zr_{0.94}Y_{0.06})_{0.2}Sn_{0.2}Ti_{0.2}Hf_{0.2}Mn_{0.2})O_{3-x}$ ,  $(Ce_{0.2}Zr_{0.2}Hf_{0.2}Sn_{0.2}Ti_{0.2})O_2$ ,  $(V_{0.2}Nb_{0.2}Ta_{0.2}Mo_{0.2}W_{0.2})C$  were observed to be entropy stabilized.<sup>[8-10]</sup> As many more ternary, quaternary, and especially non-equimolar compositions were found to have better properties, especially mechanical and thermal properties, than the equimolar composition ceramics, such as hardness, Young's moduli of  $(Hf_{0.284}Zr_{0.284}Ce_{0.284}Y_{0.074}Yb_{0.074})O_{2-δ}$  was higher than that of its equimolar counterpart and such is a case in  $(Zr_{0.225}Hf_{0.225}Ta_{0.225}Mo_{0.225}W_{0.1})B_2$  had hardness better than  $(Zr_{0.2}Hf_{0.2}Ta_{0.2}Mo_{0.2}W_{0.2})B_2$ ,<sup>[4]</sup> hence a collective term compositional complex ceramics was used to group medium

D. T. Teppala, J. Bernauer, A. Rashid, E. Ionescu  
Institute for Materials Science  
TU Darmstadt  
Otto-Berndt-Str. 3, D-64287 Darmstadt, Germany  
E-mail: emanuel.ionescu@iwks.fraunhofer.de

M. Pejic, D. Zagorac, B. Matovic  
Department of Materials Science  
Vinca Institute of Nuclear Sciences  
University of Belgrade  
Mike Petrovića Alasa 12-14, Vinča, 11351 Belgrade, Serbia

E. Ionescu  
Fraunhofer IWKS  
Brentanost. 2a, D-63755 Alzenau, Germany

 The ORCID identification number(s) for the author(s) of this article can be found under <https://doi.org/10.1002/adem.202302165>.

© 2024 The Author(s). Advanced Engineering Materials published by Wiley-VCH GmbH. This is an open access article under the terms of the Creative Commons Attribution-NonCommercial-NoDerivs License, which permits use and distribution in any medium, provided the original work is properly cited, the use is non-commercial and no modifications or adaptations are made.

DOI: 10.1002/adem.202302165

entropy, high entropy, non-equimolar compositionally complex, and entropy stabilized ceramics.<sup>[4,11,12]</sup> As the synthesis procedure developed, the research on the compositionally complex ceramics skyrocketed. Currently, various carbides such as  $(\text{Ti}_{0.2}\text{Zr}_{0.2}\text{Hf}_{0.2}\text{Nb}_{0.2}\text{Ta}_{0.2})\text{C}$ ,  $(\text{V}_{0.2}\text{Nb}_{0.2}\text{Ta}_{0.2}\text{Mo}_{0.2}\text{W}_{0.2})\text{C}$ ,  $(\text{Hf}_{0.2}\text{Nb}_{0.2}\text{Ta}_{0.2}\text{Ti}_{0.2}\text{V}_{0.2})\text{C}$ ,  $(\text{V}_{0.2}\text{Nb}_{0.2}\text{Ta}_{0.2}\text{Ti}_{0.2}\text{W}_{0.2})\text{C}$ , etc.,<sup>[6,13]</sup> nitrides such as  $(\text{V}_{0.2}\text{Cr}_{0.2}\text{Nb}_{0.2}\text{Mo}_{0.2}\text{Zr}_{0.2})\text{N}$ ,  $(\text{Ti}_{0.2}\text{Zr}_{0.2}\text{Hf}_{0.2}\text{Nb}_{0.2}\text{Ta}_{0.2})\text{N}$ ,<sup>[14,15]</sup> silicides, i.e.,  $(\text{V}_{0.2}\text{Cr}_{0.2}\text{Nb}_{0.2}\text{Ta}_{0.2}\text{W}_{0.2})\text{Si}_3$ ,  $(\text{Ti}_{0.2}\text{Zr}_{0.2}\text{Nb}_{0.2}\text{Mo}_{0.2}\text{Hf}_{0.2})\text{Si}_3$ ,<sup>[16]</sup> borides especially diborides such as  $(\text{Hf}_{0.2}\text{Zr}_{0.2}\text{Ta}_{0.2}\text{Nb}_{0.2}\text{Ti}_{0.2})\text{B}_2$ ,  $(\text{Hf}_{0.2}\text{Zr}_{0.2}\text{Ta}_{0.2}\text{Mo}_{0.2}\text{Ti}_{0.2})\text{B}_2$ ,  $(\text{Hf}_{0.2}\text{Zr}_{0.2}\text{Mo}_{0.2}\text{Nb}_{0.2}\text{Ti}_{0.2})\text{B}_2$ ,  $(\text{Hf}_{0.2}\text{Mo}_{0.2}\text{Ta}_{0.2}\text{Nb}_{0.2}\text{Ti}_{0.2})\text{B}_2$ ,  $(\text{Mo}_{0.2}\text{Zr}_{0.2}\text{Ta}_{0.2}\text{Nb}_{0.2}\text{Ti}_{0.2})\text{B}_2$ , and  $(\text{Hf}_{0.2}\text{Zr}_{0.2}\text{Ta}_{0.2}\text{Cr}_{0.2}\text{Ti}_{0.2})\text{B}_2$ ,<sup>[17]</sup> carbonitrides with equal site occupancies in the anionic sublattice  $(\text{Ti}_{0.33}\text{Zr}_{0.33}\text{Hf}_{0.33})(\text{C}_{0.5}\text{N}_{0.5})$ ,  $(\text{Ti}_{0.25}\text{Zr}_{0.25}\text{Hf}_{0.25}\text{Nb}_{0.25})(\text{C}_{0.5}\text{N}_{0.5})$  and  $(\text{Ti}_{0.2}\text{Zr}_{0.2}\text{Hf}_{0.2}\text{Nb}_{0.2}\text{Ta}_{0.2})(\text{C}_{0.5}\text{N}_{0.5})$ ,<sup>[18,19]</sup> etc. were successfully synthesized by different methods such as carbo/borothermal reductions,<sup>[8,13]</sup> spark plasma sintering (SPS),<sup>[5,8–10]</sup> magnetron sputtering,<sup>[20–22]</sup> high-pressure synthesis,<sup>[23]</sup> etc. The compositionally complex ceramics were investigated extensively and are found to have improved properties such as hardness, fracture toughness, oxidation resistance, irradiation resistance, and also better elastic moduli as compared to those of the binary ceramics due to 1) the cocktail effect; 2) the lattice distortion; as well as 3) the sluggish diffusion and high entropic effect.<sup>[1,8–11]</sup>

Although many compositions, such as oxides such as  $(\text{Mg}_{0.2}\text{Ni}_{0.2}\text{Co}_{0.2}\text{Cu}_{0.2}\text{Zn}_{0.2})\text{O}$ ,<sup>[8]</sup>  $(\text{Ce}_{0.2}\text{Zr}_{0.2}\text{Hf}_{0.2}\text{Sn}_{0.2}\text{Ti}_{0.2})\text{O}_2$ ,<sup>[9]</sup> carbides such  $(\text{Hf}_{0.2}\text{Nb}_{0.2}\text{Ta}_{0.2}\text{Ti}_{0.2}\text{Zr}_{0.2})\text{C}$ ,  $(\text{Hf}_{0.2}\text{Nb}_{0.2}\text{Ta}_{0.2}\text{Ti}_{0.2}\text{V}_{0.2})\text{C}$ ,  $(\text{Hf}_{0.2}\text{Mo}_{0.2}\text{Ta}_{0.2}\text{W}_{0.2}\text{Zr}_{0.2})\text{C}$ ,  $(\text{V}_{0.2}\text{Nb}_{0.2}\text{Ta}_{0.2}\text{Mo}_{0.2}\text{W}_{0.2})\text{C}$ <sup>[6]</sup> could be synthesized as bulk materials, metal nitrides were synthesized mainly as thin films,<sup>[20–22]</sup> as they pose significant challenges related to the synthesis procedures due to the high fugacity of nitrogen. Jin et al. synthesized  $(\text{V}_{0.2}\text{Cr}_{0.2}\text{Nb}_{0.2}\text{Mo}_{0.2}\text{Zr}_{0.2})\text{N}$  by ball milling the respective chlorides with urea followed by pyrolysis at 800 °C under  $\text{N}_2$ .<sup>[14]</sup> Moskovskikh et al. synthesized  $(\text{Ti}_{0.2}\text{Zr}_{0.2}\text{Hf}_{0.2}\text{Nb}_{0.2}\text{Ta}_{0.2})\text{N}$  by spark plasma sintering of combustion synthesized ball-milled metal powders under  $\text{N}_2$ .<sup>[15]</sup> The combustion synthesized ceramic consisted of multiple phases. However, the adiabatic combustion temperature is around 2700 °C, and the sintered samples showed oxide contaminations even after exposure to 1800 °C, and the mechanical properties surpassed the binary nitrides. Wen et al. synthesized  $(\text{Ti}_{0.2}\text{Zr}_{0.2}\text{Hf}_{0.2}\text{Nb}_{0.2}\text{Ta}_{0.2})\text{C}_{0.5}\text{N}_{0.5}$  by hot-pressing the respective ball-milled binary carbides and nitrides at 1800 °C. The prepared high-entropy carbonitride had a higher hardness and elastic moduli than their analogous high-entropy carbides and nitrides synthesized under similar conditions.<sup>[19]</sup>

Dialkylamido-based organometallic compounds have been used in chemical vapor deposition to obtain thin metal nitride films for various applications such as gas sensors, dielectric materials, and battery materials depending on the metal.<sup>[24–26]</sup> This method requires relatively low temperatures and provides nitride-based formulations with good crystallinity. The dialkylamido metal complexes can be modified by various amines, depending on the requirement for carbon (or its absence) in the final nitride-based ceramic. A high N/M ratio in the case of the metal dialkylamido complex results in a metal nitride with high nitrogen content during ammonolysis and tailorable carbon content. In the present article, we report the synthesis of a compositionally complex nitride  $(\text{Ti}_{0.2}\text{Zr}_{0.2}\text{Hf}_{0.2}\text{Nb}_{0.2}\text{Ta}_{0.2})\text{N}_x\text{C}_{1-x}$  via a

non-oxidic sol–gel method by employing transitional metal dimethyl amido complexes and a double ammonolysis process.

## 2. Experimental Section

### 2.1. Materials Synthesis

#### 2.1.1. Synthesis of Metal Dimethylamino Complexes

Chlorides of titanium, zirconium, hafnium, niobium, and tantalum, as well as lithium dimethylamide and n-hexane (anhydrous, 95%), were purchased from Merck (Germany) and stored in the glove box for further usage. All glassware used for the different steps of the synthesis procedure, including low-temperature ammonolysis, were oven dried at 120 °C at least a day to remove the adsorbed moisture. A suspended solution of 12.346 g (241 mmol) lithium dimethylamide in 60 mL hexane was prepared inside the glove box. Subsequently, 2.702 g (10 mmol) of niobium(V) chloride and 3.582 g (10 mmol) of tantalum(V) chloride were directly added into the suspension according to the procedure reported by Bradley et al.<sup>[27]</sup> The solution was stirred for 30 min until the color changed to brown. Then, it was connected to a Schlenk line and cooled to –10 °C. 2.33 g (10 mmol) zirconium(IV) chloride and 3.203 g (10 mmol) hafnium(IV) chloride were added dropwise under argon protection to prevent contact with air. Finally, a solution of 1.92 g (10.12 mmol) titanium(IV) chloride in 40 mL of hexane was added dropwise to the suspension under vigorous stirring. The reaction mixture was allowed to warm up to room temperature and was refluxed for 5 h in an argon atmosphere to ensure a complete reaction between the reagents and to avoid the formation of chlorinated metal nitrides during the ammonolysis step.<sup>[28]</sup>

Following refluxing, the resulting reddish-orange solution was cooled to room temperature, and the precipitated by-product (i.e., LiCl) was removed using filtration under argon.

#### 2.1.2. Non-Oxidic Sol–Gel Process

The filtered  $(\text{Ti,Zr,Hf,Nb,Ta})[\text{N}(\text{CH}_3)_2]_x$  solution was cooled to –72 °C and subsequently, gaseous  $\text{NH}_3$  (Air-Liquide,  $\text{O}_2 < 200$  ppm) was introduced into the reaction vessel containing the solution (see in **Figure 1**).<sup>[29,30]</sup>

The reaction solution was treated with  $\text{NH}_3$  for 5 min, resulting in a change from reddish-orange to yellowish-orange, and was eventually warmed up to room temperature. Subsequently, the solvent was removed under vacuum to obtain a slightly yellowish-brownish xerogel, which was stored in the glove box for further usage. The xerogel was observed to be pyrophoric under an ambient atmosphere.

#### 2.1.3. Ammonolysis and High-Temperature Annealing

The obtained xerogel was placed in a quartz crucible coated with a thin layer of h-BN (to prevent its reaction with the xerogel), which in turn was placed in a quartz tube. The xerogel was ammonolysed at 1000 and 1100 °C for 3 h using a flow rate of 0.3 L  $\text{min}^{-1}$  and a heating and cooling rate of 100 °C  $\text{min}^{-1}$ .

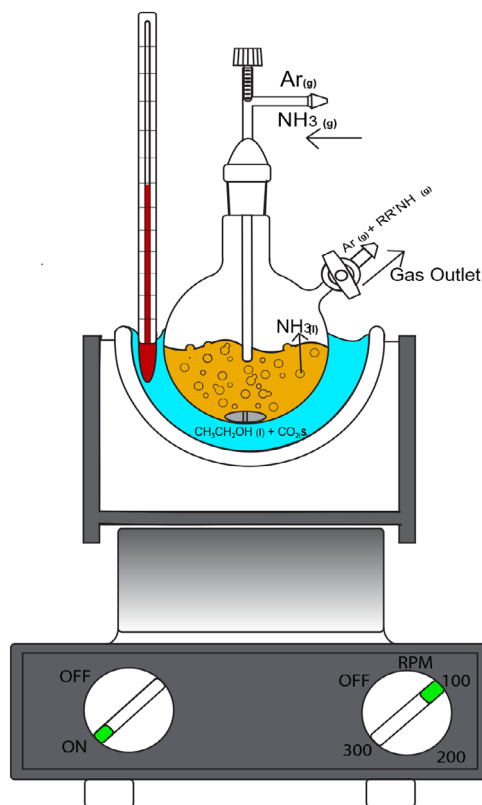


**Figure 1.** Schematics of low-temperature ammonolysis.

The ceramic powder was then placed in a graphite crucible and annealed independently at two selected temperatures, 1500 and 1700 °C, for 3 h with a heating rate of 15 °C min<sup>-1</sup> and a cooling rate of 20 °C min<sup>-1</sup> under N<sub>2</sub>. The flow rate was maintained at 1.2 L min<sup>-1</sup> for the whole duration of the thermal treatment process.

## 2.2. Characterization Techniques

The metal amido complexes and lithium dimethylamide were analyzed by using a Fourier transformed infra-red spectrometer (FTIR) in attenuated total reflection (ATR) under argon atmosphere with VARIAN-670 (Agilent Technologies) in the range of 400 to 4000 cm<sup>-1</sup> with automatic baseline and background corrections. The Raman spectra of the ceramics were measured with a Horiba Jobin Yvon HR800 spectrometer with the blue laser of wavelength 488 nm with Si as calibration standard, for 10 cycles with an acquisition time of 10 s for each cycle from the range of 0–1500 cm<sup>-1</sup> with 1800 grating. The spectra were recorded in triplicate. The thermo gravimetric analysis (TGA) was obtained from Netzsch STA 449F2 under ammonia atmosphere with a heating rate of 5 °C min<sup>-1</sup> until 1200 °C. The crystal structure and the phase composition details were obtained from XRD patterns recorded with a Huber Guinier Camera 670-360 powder XRD machine (HUBER Diffraktionstechnik GmbH, Germany) equipped with a Germanium(220) monochromator, resulting Mo-K<sub>α</sub> radiation ( $\lambda = 0.70932 \text{ \AA}$ ) in the range of 4°–100° with a step size of 0.025° and total acquisition time of

180 min to obtain high SNR. The diffractogram was analyzed with the help of MATCH! Software (Crystal Impact GmbH, Germany) and the Rietveld refinements were performed using FULLPROF<sup>[31]</sup> with Thompson Cox Hasting with Axial Divergence function until a scattering angle of 55° except for sample ammonolysed at 1100 °C. The average B<sub>iso</sub> was assumed to be isotropic. The morphology studies were performed using a Scanning Electron Microscope Philips XL30 FEG high-resolution scanning electron microscope (FEI Company, Hillsboro, Oregon, USA), coupled with an energy-dispersive X-ray (EDX) spectroscope (Mahwah, New Jersey, USA). Transmission electron microscopy (TEM) studies were performed on the powder sample calcined at 1000 °C, mildly coated with carbon to minimize electrostatic charging under the incident electron beam. Bright-field TEM (BF-TEM) as well as selected area electron diffraction (SAED) and, in addition, dark-field scanning TEM (DF-STEM) in conjunction with energy-dispersive X-ray spectroscopy (EDS) mapping for local chemical analysis, were recorded with a JEOL JEM-2100F (JEOL, Tokyo, Japan) microscope operating at 200 kV, being equipped with a CCD camera and a JEOL Be double-tilt holder for sample orientation. At the same time, EDS spectra were acquired in triplicate using an Oxford XMAX 80 detector (Oxford Instruments Nano Analysis, Wiesbaden, Germany). The elemental (C, N, O) analysis of the ceramics was performed using an LECO analyzer (LECO Corporation, St. Joseph, Michigan, USA).

## 2.3. Theoretical Investigations

The envisaged multi-component high-entropy carbonitride system (Ti<sub>0.2</sub>Zr<sub>0.2</sub>Hf<sub>0.2</sub>Nb<sub>0.2</sub>Ta<sub>0.2</sub>)C<sub>1-x</sub>N<sub>x</sub> was investigated using a multimethodological approach.<sup>[32–34]</sup> Structure candidates were explored using the primitive cell approach for atom exchange (PCAE) method,<sup>[35]</sup> the supercell approach,<sup>[33,36]</sup> special quasi-random structures (SQS),<sup>[37,38]</sup> and data mining (DM) methods.<sup>[32,39]</sup> Full structural optimizations of the models generated using supercell and SQS methods were done on the ab initio level using density functional theory (DFT) calculations within the Quantum Espresso (QE)<sup>[40]</sup> software package. Structure candidates generated using PCAE and DM methods were carried out using CRYSTAL17 code.<sup>[41]</sup> All DFT Calculations were utilized using the generalized gradient approximation (GGA) with the Perdew, Burke, and Ernzerhof (PBE) functional.<sup>[42]</sup>

QE is a code that uses plane-wave DFT, for which a 50 Ry kinetic energy cutoff for wavefunctions was used in the present investigations. In particular, the QE pseudopotentials used in this study are the following: Hf.pbe-spn-kjpaw\_psl.1.0.0.UPF, Zr.pbe-spn-kjpaw\_psl.1.0.0.UPF, Ti.pbe-spn-kjpaw\_psl.1.0.0.UPF, Ta.pbe-spn-kjpaw\_psl.1.0.0.UPF, Nb.pbe-spn-kjpaw\_psl.1.0.0.UPF, N.pbe-n-kjpaw\_psl.1.0.0.UPF, C.pbe-n-kjpaw\_psl.1.0.0.UPF, for Hf, Zr, Ti, Ta, Nb, N, and C, respectively.<sup>[43]</sup> A convergence tolerance of 10<sup>-8</sup> for the structure relaxation was chosen.

As for the Crystal17 code, based on the linear combination of atomic orbitals, for calculations with 8 × 8 × 8 K-point mesh using the Monkhorst–Pack scheme, various basis sets (BS) were used: BS for zirconium denoted as Zr ECP HAYWSC 311d31G dovesi 1998,<sup>[44,45]</sup> BS for hafnium Hf ECP Stevens 411d31G munoz 2007,<sup>[45,46]</sup> BS for titanium labeled Ti\_86–51(3d)

G\_muscat\_1999,<sup>[46]</sup> BS for niobium Nb\_SC\_HAYWSC-31(31d) G\_baranek\_2013,<sup>[47]</sup> for tantalum Ta\_ECP60MDF-31(51df)G\_baranek\_2013,<sup>[48]</sup> for carbon C\_6-21G\*\_catti\_1993<sup>[49]</sup> and a modified BS for nitrogen N\_6-31d1G\_gatti\_1994.<sup>[50]</sup>

The symmetry of computed and predicted models was analyzed using the SFND algorithm<sup>[51]</sup> and RGS algorithm<sup>[52]</sup> implemented in the KPLOT software,<sup>[53]</sup> while structures were visualized using the VESTA code.<sup>[54]</sup>

### 3. Results and Discussion

#### 3.1. Synthesis of Multimetal Dimethylamido Complexes

The (Ti,Zr,Hf,Nb,Ta) dimethylamide precursor was synthesized as yellowish-orange xerogel. The FTIR data of the xerogel are shown in Figure 2.

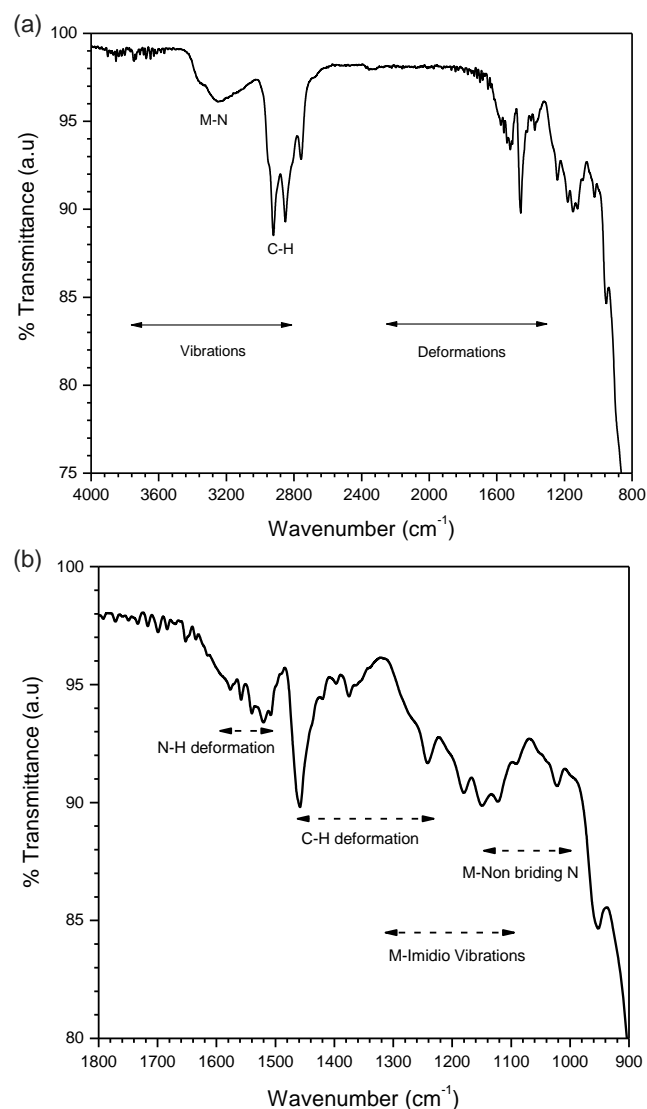


**Figure 2.** a) FTIR of xerogel (Ti,Zr,Hf,Nb,Ta)[(μ-NH)<sub>x</sub>(NH<sub>2</sub>)<sub>y</sub>(N(CH<sub>3</sub>)<sub>2</sub>)<sub>z</sub>]. Plot in b) represents the magnified spectrum in the region from 900 to 1800 cm<sup>-1</sup>.

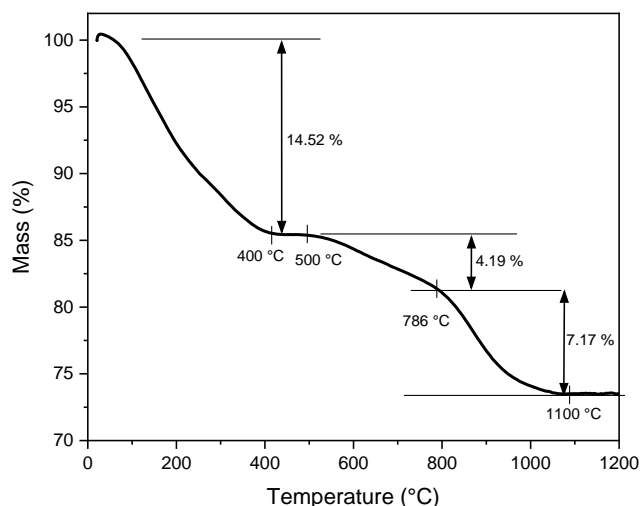


**Figure 3.** TGA data of (Ti,Zr,Hf,Nb,Ta)[(μ-NH)<sub>x</sub>(NH<sub>2</sub>)<sub>y</sub>(N(CH<sub>3</sub>)<sub>2</sub>)<sub>z</sub> measured up to 1200 °C under NH<sub>3</sub>.

The IR bands in the range of 3100–3600 cm<sup>-1</sup> correspond to the N–H vibrations along with the deformation bands of N–H between 1500 to 1575 cm<sup>-1</sup>.<sup>[55,56]</sup> The bands with minima positioned around 2900 cm<sup>-1</sup> are allocated to the C–H stretching, and C–H deformation bands were located in the range of 1230–1489 cm<sup>-1</sup>.<sup>[56,57]</sup> Metal imido vibrations were assigned to the bands in the range of 1100 till 1300 and 1000–1150 cm<sup>-1</sup> to metal non-bridging nitrogen, suggesting that the obtained xerogel consists of M–N, N–H, N(CH<sub>3</sub>) bonds, with the possibility of xerogel being an oligomer.<sup>[30]</sup>

The TGA results of the xerogel performed under ammonia consist of a plateau region from 400 to 500 °C (see Figure 3). The considerable mass loss of 14.5% corresponds to the evolution of N(CH<sub>3</sub>)<sub>2</sub>H, NH<sub>3</sub>, and N<sub>2</sub>, as shown for similar xerogels based on transitional metal amido complexes exposed to thermal ammonolysis conditions.<sup>[30,56]</sup> The additional mass loss of ≈12% up to 1100 °C corresponds to the decomposition of nitrogen-rich phase(s) into mono-nitride phase.<sup>[56]</sup>

#### 3.2. Ammonolysis and High-Temperature Annealing

Figure 4 shows the XRD pattern of the ammonolyzed xerogel at 1000 °C. The obtained ceramic is crystalline, showing (TiZrHfNbTa)N with a rock salt structure (Fm-3m) as main phase and two minor phases, which were assigned to zirconium oxides with monoclinic (P2<sub>1</sub>/c), i.e., Baddeleyite and tetragonal (P4<sub>2</sub>/nmc) structures along with Ta<sub>3</sub>N<sub>5</sub> orthorhombic (Cmcm) structure.

The xerogel was also ammonolyzed at 1100 °C to observe the stability of the minor secondary phases. It was observed that the Ta<sub>3</sub>N<sub>5</sub>-based Cmcm phase had disappeared, but the oxide impurities were stable in a P2<sub>1</sub>/c-based monoclinic structure. The Rietveld analysis of the XRD pattern in Figure 5 resulted in a lattice parameter of 4.28 Å with ≈10 wt% of oxide impurity for the sample ammonolyzed at 1100 °C, compared to the lattice parameter 4.26 Å of the nitride phase obtained at 1000 °C (Figure 6).

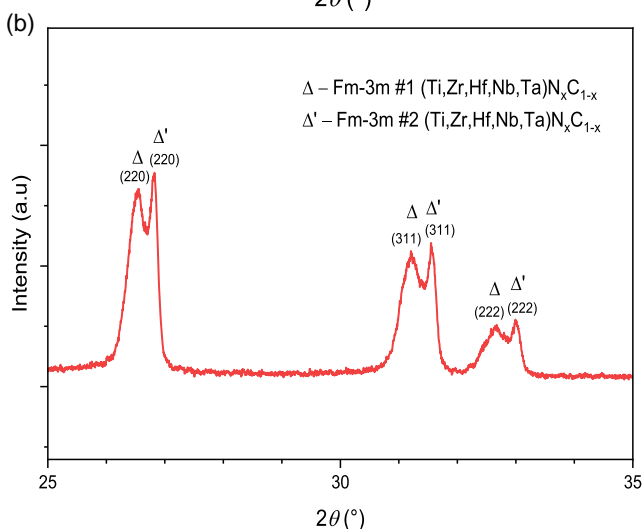
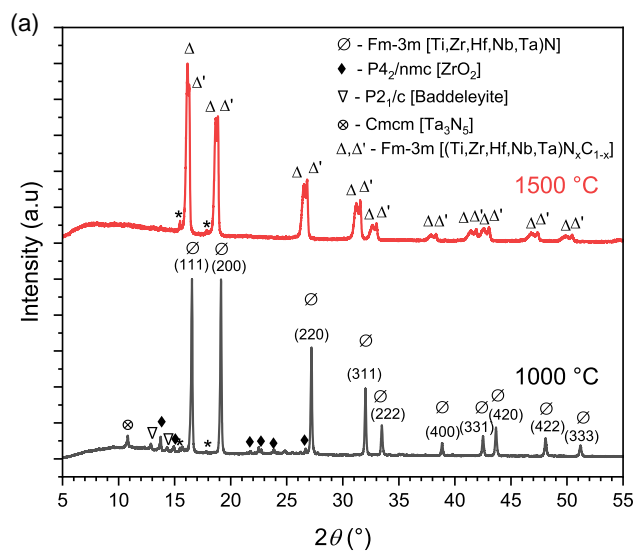


**Figure 4.** a) XRD patterns of  $(\text{Ti,Zr,Hf,Nb,Ta})\text{N}_x\text{C}_{1-x}$  prepared via ammonolysis at 1000 °C (bottom) and subsequently annealed in nitrogen atmosphere at 1500 °C (top). In b), the 2theta region from 25° to 35° of the diffractogram of the sample prepared at 1500 °C is shown. (Peaks labeled with \*correspond to instrumental artifacts).

However, in the case of the sample annealed at 1500 °C, there were no reflections corresponding to oxides (see Figure 4a). Interestingly, the reflections corresponding to the rock salt-type nitride phase were considerably shifted toward lower diffraction angles. Moreover, two sets of reflections corresponding to rock salt structure have been detected (see Figure 4b). From these observations, it is concluded that carbon diffusion into the high-entropy metal nitride structure may have occurred upon annealing at 1500 °C due to the graphite crucible acting as a carbon source. Consequently, the minor oxide phases are also expected to be converted into a compositionally complex carbonitride. Moreover, spinodal decomposition may be possible, with both rock-salt-type phases being either nitride or carbonitride with different cationic and anionic sublattice occupancies.<sup>[58]</sup> Additionally, the dissolution of the oxygen into the compositionally complex (carbo)nitrides cannot be excluded as

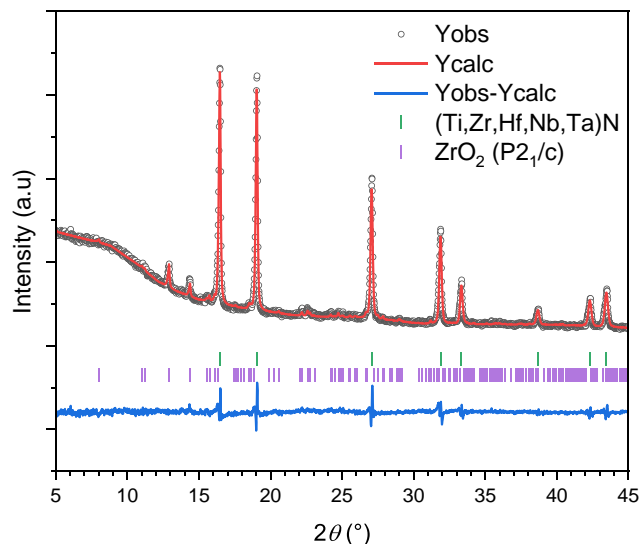


**Figure 5.** Rietveld of  $(\text{Ti,Zr,Hf,Nb,Ta})\text{N}$  obtained after ammonolysis at 1100 °C.

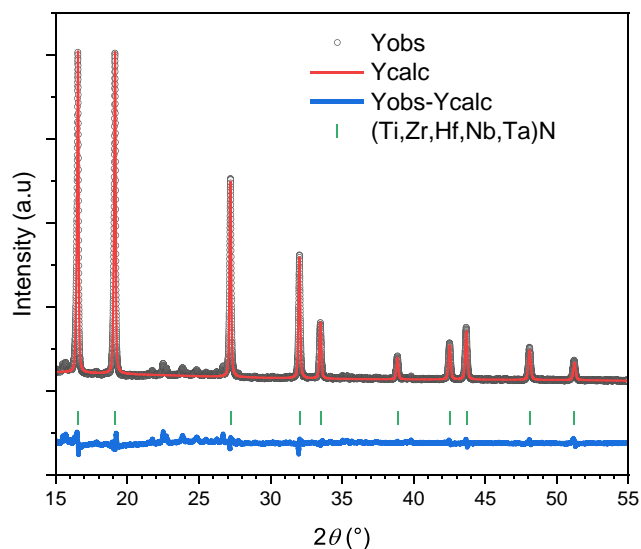


**Figure 6.** Rietveld of  $(\text{Ti,Zr,Hf,Nb,Ta})\text{N}$  obtained after ammonolysis at 1000 °C.

the native oxide cannot be reduced entirely by carbothermal reductions.<sup>[59–61]</sup>

The Rietveld analysis of the 1500 °C annealed ceramic (see Figure 7) revealed the lattice parameters of the two phases to be 4.37 Å for phase *Fm-3m* #1 and 4.32 Å for phase *Fm-3m* #2. The phases were present with a molar ratio of 3:1.

### 3.3. Phase Evolution upon Annealing at 1700 °C under $\text{N}_2$

As the annealing temperature was increased to 1700 °C, a single-phase ceramic  $(\text{Ti,Zr,Hf,Nb,Ta})\text{N}_x\text{C}_{1-x}$  was obtained. This ceramic showed a considerable shift in the lattice parameter as compared to the two rock-salt phases observed in the ceramic



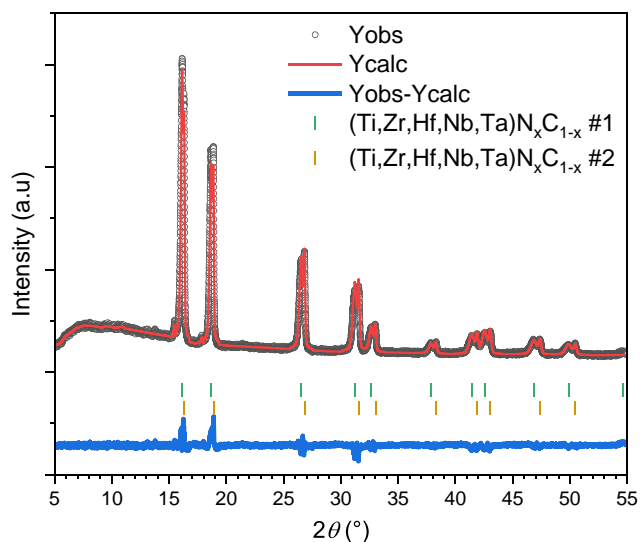


**Figure 7.** Rietveld refinement of  $(\text{Ti}_{0.2}\text{Zr}_{0.2}\text{Hf}_{0.2}\text{Nb}_{0.2}\text{Ta}_{0.2})\text{N}_x\text{C}_{1-x}$  annealed at 1500 °C using linear interpolation as background.

annealed at 1500 °C, suggesting that carbon has been incorporated into the structure.

The Rietveld refinement of the XRD pattern obtained from the single-phase  $(\text{Ti,Zr,Hf,Nb,Ta})\text{N}_x\text{C}_{1-x}$  annealed at 1700 °C indicated a lattice parameter of 4.39 Å (Figure 8).

Depending on the carbon and nitrogen contents, the synthesized ceramics are expected to have slightly smaller lattice parameters than the stoichiometric compositions.<sup>[62,63]</sup>

### 3.4. Chemical Composition of the Ceramics

The elemental analysis of the sample ammonolyzed at 1000 °C indicated a carbon-free composition with a nitrogen content of ≈8.6 wt%; while the oxygen content was ≈2.1 wt%, suggesting the presence minor amount of oxide phase(s) in the main phase,

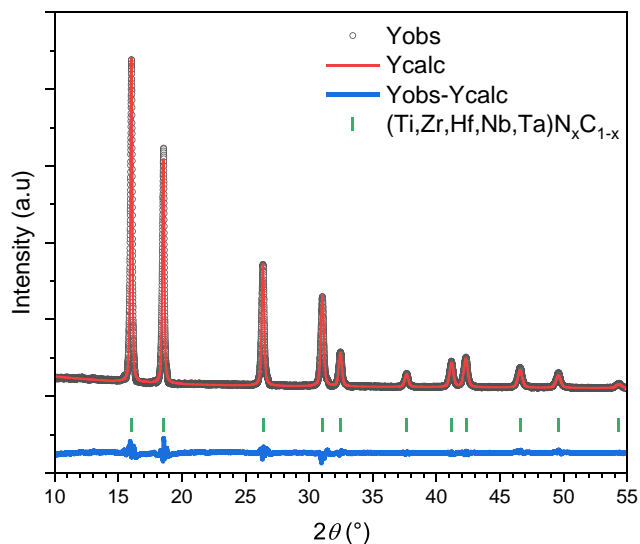


**Figure 8.** Rietveld profile of  $(\text{Ti,Zr,Hf,Nb,Ta})\text{N}_x\text{C}_{1-x}$  annealed at 1700 °C.

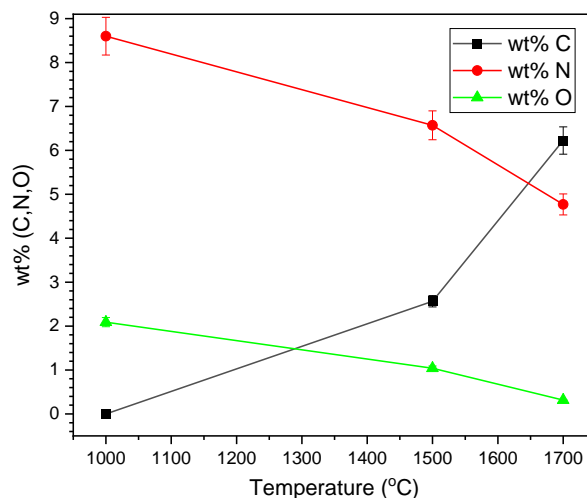


**Figure 9.** The carbon, nitrogen, and oxygen content of ceramic prepared at 1000 °C, including the samples, annealed at 1500 and 1700 °C under  $\text{N}_2$ .

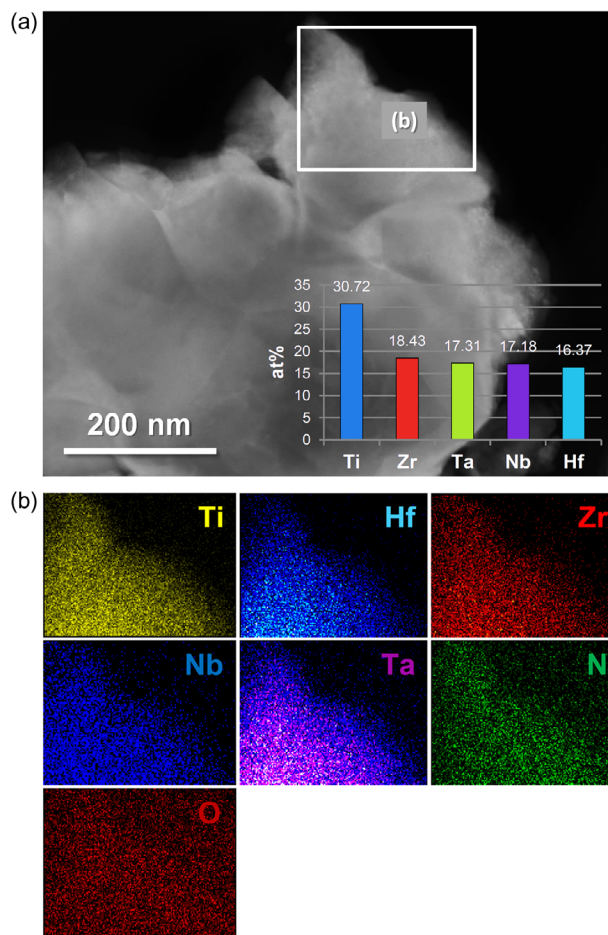


**Figure 10.** a) BF-TEM image of the ceramic prepared upon ammonolysis at 1000 °C. In the inset, the relative contents of the metallic elements are indicated; those were determined by energy-dispersive X-ray spectroscopy (EDS); b) EDS maps (DF-STEM, corresponding to area (b) in (a)) showing the homogeneous distribution of the five transitional metals within an individual grain.

i.e., compositionally complex metal nitride. Annealing in nitrogen atmosphere at 1500 and 1700 °C leads to a decrease of the oxygen content to  $\approx 1$  and 0.3 wt%, respectively; whereas the exposure to high temperatures induced the diffusion of carbon into the structure of the metal nitride, leading to carbon contents of 2.4 and 6.2 wt% upon annealing to 1500 and 1700 °C, respectively. As the same time, the nitrogen content in the samples annealed at 1500 and 1700 °C decreased to 6.6 and 4.8 wt%, respectively (Figure 9).

Using the aforementioned data as well as the metal contents determined by means of EDS (see Figure 10a), the composition of the ceramic samples prepared at 1000, 1500, and 1700 °C were calculated as  $(\text{Ti}_{0.31}\text{Zr}_{0.19}\text{Hf}_{0.16}\text{Nb}_{0.17}\text{Ta}_{0.17})(\text{N}_{0.74}\text{O}_{0.18})$ ,  $(\text{Ti}_{0.31}\text{Zr}_{0.19}\text{Hf}_{0.16}\text{Nb}_{0.17}\text{Ta}_{0.17})(\text{N}_{0.56}\text{C}_{0.2}\text{O}_{0.09})$  and  $(\text{Ti}_{0.31}\text{Zr}_{0.19}\text{Hf}_{0.16}\text{Nb}_{0.17}\text{Ta}_{0.17})(\text{N}_{0.42}\text{C}_{0.54}\text{O}_{0.03})$ , respectively.

In order to rationalize the reliability of the elemental composition of the prepared (carbo)nitrides, three additional successive batches of carbonitride were prepared at 1700 °C. The elemental composition of the three batches was determined by EDS (10 measurements per batch) and resulted in an average elemental composition of  $(\text{Ti}_{0.18\pm 0.072}\text{Zr}_{0.20\pm 0.024}\text{Hf}_{0.20\pm 0.01}\text{Nb}_{0.22\pm 0.03}\text{Ta}_{0.20\pm 0.016})(\text{N}_{0.40\pm 0.016}\text{C}_{0.51\pm 0.02}\text{O}_{0.06\pm 0.01})$ .

While the carbon, nitrogen, and oxygen content of the different synthesized batches were very consistent, showing only low fluctuation, the elemental composition of the metals seems to exhibit higher fluctuation. For instance, the scattering of the atomic fraction of Ti seems to be correlated to the stronger variation in its content among the different synthesized batches

(i.e., compare the composition  $\text{Ti}_{0.31}\text{Zr}_{0.19}\text{Hf}_{0.16}\text{Nb}_{0.17}\text{Ta}_{0.17}$  from the first batch with the average composition  $\text{Ti}_{0.18\pm 0.072}\text{Zr}_{0.20\pm 0.024}\text{Hf}_{0.20\pm 0.01}\text{Nb}_{0.22\pm 0.03}\text{Ta}_{0.20\pm 0.016}$  from the subsequent three batches). This aspect has been currently under investigation.

### 3.5. Theoretical Study of the HEA Carbonitride Systems

A large number of supercell and SQS structures were generated to investigate the stable phases of high-entropy nitride and carbonitride structures. The most promising candidates are shown in Figure 11a–c. The most stable phase appears in the rock-salt type of structure with cubic symmetry ( $Fm\bar{3}m$  space group) in both compositionally complex nitride (HEN) and high-entropy carbonitride (HECN) depicted in Figure 11a. This is in agreement with our experimental observation where several cubic ( $Fm\bar{3}m$  space group) have been observed. The origin of the rock salt HEN/HECN structure can be derived from the TaN prototype B1 structure.<sup>[64]</sup> Present GGA-PBE calculations on the SQS cubic HEN model results in  $a = 4.445 \text{ \AA}$  (compared to the experimental value of both cubic rock-salt phases 1#  $a = 4.3698 \text{ \AA}$  and #2  $a = 4.3334 \text{ \AA}$  at 1500 °C) and for the SQS cubic HECN model results in  $a = 4.490 \text{ \AA}$  (compared to the experimental value of  $a = 4.39 \text{ \AA}$  at 1700 °C), which is in an excellent agreement with experimental XRD results.

In addition, we predict two novel SQS supercell models in compositionally complex carbonitride computed using DFT. Figure 11b shows a hexagonal-1 phase with space group

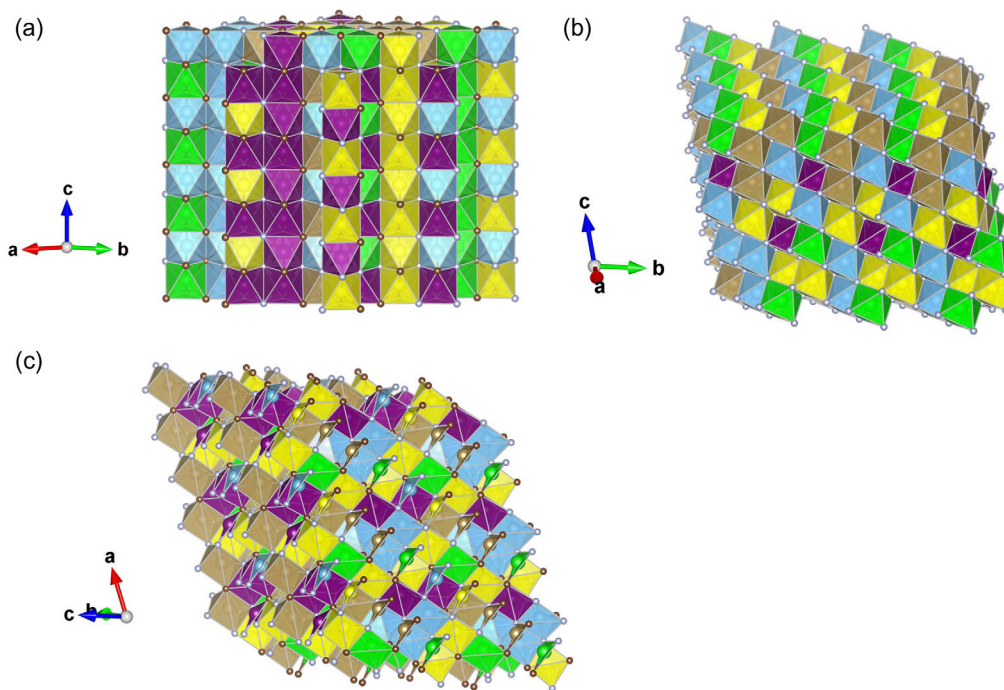


**Figure 11.** Picture of the energetically most favorable found SQS supercell structures of the high-entropy (carbo)nitride with the: a) cubic rock-salt type ( $Fm\bar{3}m$  space group) phase of the HE nitride, b) hexagonal-1 ( $P\bar{6}2m$ ) phase of the HE carbonitrides, c) hexagonal-2 ( $P63mc$ ) phase of the HECN, shown with coordination polyhedra around the metal atoms. Green balls correspond to Zr atoms, light brown correspond to Ta atoms, blue correspond to Ti atoms, yellow correspond to Nb atoms, purple correspond to Hf atoms, grey balls correspond to nitrogen atoms, and dark brown balls correspond to carbon atoms, respectively.

$P-62m$  in the HECN system, originating from the distorted hexagonal TaN prototype.<sup>[65]</sup> The hexagonal-2 modification also with the HECN composition is presented in Figure 11c. The predicted hexagonal-2 phase appears in space group  $P63mc$  originating from the distorted hexagonal MoN prototype.<sup>[66]</sup> We note that the hexagonal 1 modification is more stable in HEN compared to the second phase, while it is vice-versa in the case of the HECN composition.

One should not rely on randomly populating a supercell with the alloyed elements since there is a number of possible permutations in a high entropy material that can be feasibly modeled using DFT.<sup>[67]</sup> Figure 12 shows the most stable HEN/HECN predicted structures generated from the data mining and PCAE method. The layered HEN appears in the trigonal-rhombohedral ( $R3m$ ) space group of the HEN generated using the PCAE method and it could be an interesting candidate between cubic and hexagonal predicted and observed phases in the compositionally complex carbonitrides. Figure 12b shows the mono HEN phase appearing as a distorted rock-salt in the  $Cm$  monoclinic space group. This was one of the most stable modifications in the HEN system originating from the PdD prototype.<sup>[68]</sup> Similarly, the mono HECN modification with the  $Cm$  monoclinic

symmetry appears in the HECN chemical system (Figure 12c), originating from the distorted NiGa modification.<sup>[69]</sup> Both monoclinic predicted compositionally complex (carbo)nitride structures might be also interesting from the experimental point of view, since in the present study monoclinic metal oxide structures have been found as minor phases.

#### 4. Conclusion

In the current work, a straightforward method to achieve compositionally complex (carbo)nitrides was employed for the first time through non-oxidic sol-gel of multiple metal dimethylamino complexes. The ammonolysis of the xerogel at 1000 °C resulted in a single-phase compositionally complex nitride with minor amounts of oxide phases and further led to the formation of carbon-rich (carbo)nitride upon annealing at higher temperatures, with a gradual change in carbon oxygen and nitrogen contents, which were thoroughly characterized structurally by XRD chemically and morphologically through SEM. The carbon-rich carbonitride obtained via annealing at 1700 °C was phase pure with a nearly homogenous composition of the transitional

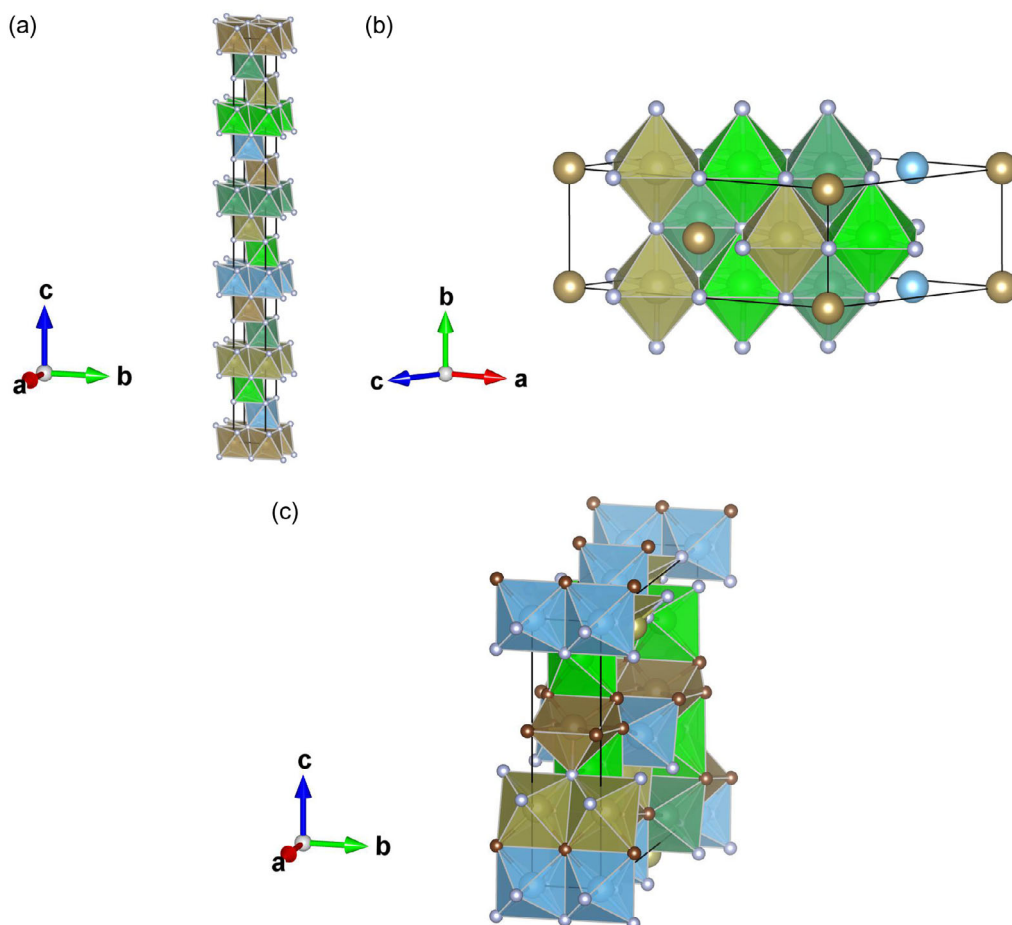


**Figure 12.** Picture of the most favorable structures found using data mining and PCAE method of the high-entropy (carbo)nitride with the: a) layered HEN, trigonal-rhombohedral ( $R3m$  space group) phase of the nitride, b) mono HEN ( $Cm$ ) monoclinic phase of the high-entropy nitride, c) mono HECN ( $Cm$ ) phase of the HE carbonitrides, shown with coordination polyhedra around the metal atoms.



elements with anion sublattice occupancy of less than 1. Theoretical investigations were performed using the multi-methodological approach involving several computational methods. Structures were generated using the PCAE, supercell, SQS, and data mining approaches, and the ab initio DFT-PBE structure optimization results are in good agreement with experimentally obtained XRD data. Thus, the multi-methodological approach employed to model compositionally complex ceramics can be utilized to screen the formability of novel compositionally complex ceramic compositions.

## Supporting Information

Supporting Information is available from the Wiley Online Library or from the author.

## Acknowledgements

Prof. Hans-Joachim Kleebe (TU Darmstadt) is gratefully acknowledged for the (S)TEM measurements as well as for his continuous support of our research within the last two decades. DTT acknowledges DAAD for funding doctoral studies through the “Research Grants-Doctoral Programmes in Germany” scholarship. The authors acknowledge further funding from DAAD within the frame of the Programs for Project-Related Personal Exchange (PPP, project no. 57601381, “Compositionally Complex Metal Carbides and Carbonitrides”). This research was also funded by the Ministry of Science, Technological Development and Innovation of the Republic of Serbia through contract no. 451-03-47/2023-01/200017. Also, funding from the German Research Foundation (Deutsche Forschungsgemeinschaft, DFG) within the Research training Group RTG 2561 (project no. 413956820, “Materials Compounds from Composite Materials”) has been received.

Open Access funding enabled and organized by Projekt DEAL.

## Conflict of Interest

The authors declare no conflict of interest.

## Data Availability Statement

The data that support the findings of this study are available from the corresponding author upon reasonable request.

## Keywords

ammonolysis, compositional complexity, DFT, modeling, nitrides

Received: December 17, 2023

Revised: May 13, 2024

Published online: June 8, 2024

- [1] J. W. Yeh, Y. L. Chen, S. J. Lin, S. K. Chen, *Mater. Sci. Forum* **2007**, 560.  
 [2] B. Cantor, I. T. H. Chang, P. Knight, A. J. B. Vincent, *Mater. Sci. Eng. A* **2004**, 375–377, 213.  
 [3] B. Wu, Y. Zhao, H. Ali, R. Chen, H. Chen, J. Wen, Y. Liu, L. Liu, K. Yang, L. Zhang, Z. He, Q. Yao, H. Zhang, B. Sa, C. Wen, Y. Qiu, H. Xiong, M. Lin, Y. Liu, C. Wang, H. Su, *Intermetallics* **2022**, 144, 107489.

- [4] A. J. Wright, J. Luo, *J. Mater. Sci.* **2020**, 55, 9812.  
 [5] W. Hume-Rothery, H. M. Powell, *Zeitschrift Für Krist.: Cryst. Mater.* **1935**, 91, 23.  
 [6] P. Sarker, T. Harrington, C. Toher, C. Oses, M. Samiee, J.-P. Maria, D. W. Brenner, K. S. Vecchio, S. Curtarolo, *Nat. Commun.* **2018**, 9, 4980.  
 [7] C. M. Rost, E. Sachet, T. Borman, A. Moballeghe, E. C. Dickey, D. Hou, J. L. Jones, S. Curtarolo, J.-P. Maria, *Nat. Commun.* **2015**, 6, 8485.  
 [8] M. Biesuz, S. Fu, J. Dong, A. Jiang, D. Ke, Q. Xu, D. Zhu, M. Bortolotti, M. J. Reece, C. Hu, S. Grasso, *J. Asian Ceram. Soc.* **2019**, 7, 127.  
 [9] K. Chen, X. Pei, L. Tang, H. Cheng, Z. Li, C. Li, X. Zhang, L. An, *J. Eur. Ceram. Soc.* **2018**, 38, 4161.  
 [10] T. J. Harrington, J. Gild, P. Sarker, C. Toher, C. M. Rost, O. F. Dippo, C. McElfresh, K. Kaufmann, E. Marin, L. Borowski, P. E. Hopkins, J. Luo, S. Curtarolo, D. W. Brenner, K. S. Vecchio, *Acta Mater.* **2019**, 166, 271.  
 [11] M. Xia, N. Lu, Y. Chen, B. Shen, X. Liang, *Int. J. Refract. Met. Hard Mater.* **2022**, 107, 105859.  
 [12] Z. Zhang, S. Zhu, Y. Liu, L. Liu, Z. Ma, *J. Eur. Ceram. Soc.* **2022**, 42, 5303.  
 [13] Y. Wang, *Adv. Appl. Ceram.* **2022**, 121, 57.  
 [14] T. Jin, X. Sang, R. R. Unocic, R. T. Kinch, X. Liu, J. Hu, H. Liu, S. Dai, *Adv. Mater.* **2018**, 30, 1707512.  
 [15] D. Moskovskikh, S. Vorotilo, V. Buinevich, A. Sedegov, K. Kuskov, A. Khort, C. Shuck, M. Zhukovskiy, A. Mukasyan, *Sci. Rep.* **2020**, 10, 19874.  
 [16] S. Shivakumar, M. Qin, D. Zhang, C. Hu, Q. Yan, J. Luo, *Scr. Mater.* **2022**, 212, 114557.  
 [17] J. Gild, Y. Zhang, T. Harrington, S. Jiang, T. Hu, M. C. Quinn, W. M. Mellor, N. Zhou, K. Vecchio, J. Luo, *Sci. Rep.* **2016**, 6, 37946.  
 [18] P. Zhang, X. Liu, A. Cai, Q. Du, X. Yuan, H. Wang, Y. Wu, S. Jiang, Z. Lu, *Sci. China Mater.* **2021**, 64, 2037.  
 [19] T. Wen, B. Ye, M. C. Nguyen, M. Ma, Y. Chu, *J. Am. Ceram. Soc.* **2020**, 103, 6475.  
 [20] J. Li, Y. Chen, Y. Zhao, X. Shi, S. Wang, S. Zhang, *J. Alloys Compd.* **2022**, 926, 166807.  
 [21] Y. C. Lin, S. Y. Hsu, Y. T. Lai, P. H. Kuo, S. Y. Tsai, J. G. Duh, *Mater. Chem. Phys.* **2021**, 274, 125195.  
 [22] S. Y. Hsu, Y. T. Lai, S. Y. Chang, S. Y. Tsai, J. G. Duh, *Surf. Coat. Technol.* **2022**, 442, 128564.  
 [23] S. Iwan, K. C. Burrage, B. C. Storr, S. A. Catledge, Y. K. Vohra, R. Hrubiak, N. Velisavljevic, *AIP Adv.* **2021**, 11, 035107.  
 [24] Q. Xie, D. Deduytsche, J. Musschoot, R. L. V. Meirhaeghe, C. Detavernier, S. F. Ding, X. P. Qu, *Microelectron. Eng.* **2011**, 88, 646.  
 [25] J. Musschoot, Q. Xie, D. Deduytsche, S. Van den Berghe, R. L. Van Meirhaeghe, C. Detavernier, *Microelectron. Eng.* **2009**, 86, 72.  
 [26] A. Kafzas, C. J. Carmalt, I. P. Parkin, *Coord. Chem. Rev.* **2013**, 257, 2073.  
 [27] D. C. Bradley, I. M. Thomas, *J. Chem. Soc.* **1960**, 3857.  
 [28] I. P. Parkin, A. T. Rowley, *J. Mater. Chem.* **1995**, 5, 909.  
 [29] T. R. Cundari, J. M. Morse, *Chem. Mater.* **1996**, 8, 189.  
 [30] G. M. Brown, L. Maya, *J. Am. Ceram. Soc.* **1988**, 71, 78.  
 [31] J. Rodriguez-Carvajal, in *Abstract of the Satellite Meeting on Powder Diffraction of the XV Congress of the IUCr*, Toulouse, France, **1990**, p. 127.  
 [32] D. Zagorac, J. Zagorac, M. Fonović, M. Pejić, J. C. Schön, *Zeitschrift Fur Anorg. Und Allg. Chem.* **2022**, 648, e202200198.  
 [33] B. Matović, D. Zagorac, I. Cvijović-Alagić, J. Zagorac, S. Butulija, J. Erčić, O. Hanzel, R. Sedlák, M. Lisnichuk, P. Tatarko, *Boletín La Soc. Española Cerámica y Vidr.* **2023**, 62, 66.  
 [34] J. Zagorac, D. Zagorac, V. Šrot, M. Randelović, M. Pejić, P. A. van Aken, B. Matović, J. C. Schön, *Materials* **2023**, 16, 326.

- [35] D. Zagorac, J. Zagorac, J. C. Schön, N. Stojanović, B. Matović, *Acta Crystallogr. Sect. B* **2018**, *74*, 628.
- [36] D. Zagorac, K. Doll, J. C. Schön, M. Jansen, *Chem.: A Eur. J.* **2012**, *18*, 10929.
- [37] S.-H. Wei, L. G. Ferreira, J. E. Bernard, A. Zunger, *Phys. Rev. B* **1990**, *42*, 9622.
- [38] A. Zunger, S.-H. Wei, L. G. Ferreira, J. E. Bernard, *Phys. Rev. Lett.* **1990**, *65*, 353.
- [39] T. Škundrić, B. Matović, A. Zarubica, J. Zagorac, P. Tatarko, D. Zagorac, *Materials* **2021**, *14*, 7887.
- [40] P. Giannozzi, S. Baroni, N. Bonini, M. Calandra, R. Car, C. Cavazzoni, D. Ceresoli, G. L. Chiarotti, M. Cococcioni, I. Dabo, A. Dal Corso, S. de Gironcoli, S. Fabris, G. Fratesi, R. Gebauer, U. Gerstmann, C. Gougoussis, A. Kokalj, M. Lazzeri, L. Martin-Samos, N. Marzari, F. Mauri, R. Mazzarello, S. Paolini, A. Pasquarello, L. Paulatto, C. Sbraccia, S. Scandolo, G. Sclauzero, A. P. Seitsonen, et al. *J. Phys.: Condens. Matter* **2009**, *21*, 395502.
- [41] R. Dovesi, A. Erba, R. Orlando, C. M. Zicovich-Wilson, B. Civalleri, L. Maschio, M. Rérat, S. Casassa, J. Baima, S. Salustro, B. Kirtman, *WIREs Comput. Mol. Sci.* **2018**, *8*, e1360.
- [42] J. P. Perdew, K. Burke, M. Ernzerhof, *Phys. Rev. Lett.* **1996**, *77*, 3865.
- [43] A. Dal Corso, *Comput. Mater. Sci.* **2014**, *95*, 337.
- [44] T. Bredow, M. Lerch, Z. Anorg, *Allg. Chem.* **2004**, *630*, 2262.
- [45] B. Matović, J. Maletaškić, V. Maksimović, S. P. Dimitrijević, B. Todorović, M. Pejić, D. Zagorac, J. Zagorac, Y.-P. Zeng, I. Cvijović-Alagić, *Bol. Soc. Esp. Cerám. Vidr.* **2023**, *62*, 515.
- [46] D. Munoz-Ramo, J. L. Gavartin, A. L. Shluger, *Phys. Rev. B* **2007**, *75*, 205336.
- [47] I. Cvijović-Alagić, M. Rakin, S. Laketić, D. Zagorac, *Mater. Charact.* **2020**, *169*, 110635.
- [48] G. Sophia, P. Baranek, C. Sarrazin, M. Rerat, R. Dovesi, *Phase Transition* **2014**, *86*, 1069.
- [49] M. Catti, A. Pavese, R. Dovesi, *Phys. Rev. B* **1993**, *47*, 9189.
- [50] D. Zagorac, J. Zagorac, M. Fonović, T. Prikhna, B. Matović, *Int. J. Appl. Ceram. Technol.* **2023**, *20*, 174.
- [51] R. Hundt, J. C. Schön, A. Hannemann, M. Jansen, *J. Appl. Crystallogr.* **1999**, *32*, 413.
- [52] A. Hannemann, R. Hundt, J. C. Schön, M. Jansen, *J. Appl. Crystallogr.* **1998**, *31*, 922.
- [53] R. Hundt, in *KPLOT Program for Plotting and Analyzing Crystal Structures*, Technicum Scientific Publishing, Stuttgart, Germany **2016**.
- [54] K. Momma, F. Izumi, *J. Appl. Crystallogr.* **2008**, *41*, 653.
- [55] K. Nakamoto, in *Infrared and Raman Spectra of Inorganic and Coordination Compounds: Part A: Theory and Applications in Inorganic Chemistry*, 6th edition **2008**.
- [56] D. V. Baxter, M. H. Chisholm, G. J. Gama, V. F. DiStasi, A. L. Hector, I. P. Parkin, *Chem. Mater.* **1996**, *8*, 1222.
- [57] D. C. Bradley, M. H. Gitlitz, *J. Chem. Soc. A* **1969**, 980.
- [58] W. Zhang, K. Li, L. Chen, Z. Shi, S. Huo, B. Wei, S. J. L. Kang, Y. Wang, Y. Zhou, *J. Eur. Ceram. Soc.* **2023**, *44*, 1396.
- [59] P. Constant, K. Kieffer, R. Etmayer, *Monatshefte Fur Chem.* **1975**, *106*, 973.
- [60] K. Constant, R. Kieffer, P. Etmayer, *Monatshefte Für Chem.* **1975**, *106*, 823.
- [61] J. David, G. Trolliard, M. Gendre, A. Maître, *J. Eur. Ceram. Soc.* **2013**, *33*, 165.
- [62] M. Stoehr, C. S. Shin, I. Petrov, J. E. Greene, *J. Appl. Phys.* **2011**, *110*, 083503.
- [63] S. Nagakura, S. Oketani, *Trans. Iron Steel Inst. Jpn.* **1968**, *8*, 265.
- [64] J. Gatterer, G. Dufek, P. Etmayer, R. Kieffer, *Monatshefte für Chem.* **1975**, *106*, 1137.
- [65] A. N. Christensen, B. Lebeck, *Acta Cryst.* **1978**, *B34*, 261.
- [66] A. Bezinge, K. Yvon, J. Muller, W. Lengueur, P. Etmayer, *Solid State Commun.* **1987**, *63*, 141.
- [67] *High-Entropy Materials: Theory, Experiments, and Applications* (Eds: J. Brechtel, P.K. Liaw), Springer, Cham **2022**.
- [68] E. Wu, S. J. Kennedy, E. M. A. Gray, E. H. Kisi, *J. Phys.: Condens. Matter* **1996**, *8*, 2807.
- [69] M. K. Bhargava, K. Schubert, *J. Less Common Met.* **1974**, *38*, 177.